NASA Technical Memorandum 81411

(NASA-TM-81411) NUMERICAL SIMULATION OF SUPERSONIC INLETS USING A THREE-DIMENSIONAL VISCOUS FLOW ANALYSIS (NASA) 17 p
HC A02/MF A01 CSCL 20D G3/34

N80-15365
Unclas
46643

NUMERICAL SIMULATION OF SUPERSONIC INLETS USING A THREE-DIMENSIONAL VISCOUS FLOW ANALYSIS

B. H. Anderson and C. E. Towne
Lewis Research Center
Cleveland, Ohio

Prepared for the
Eighteenth Aerospace Sciences Meeting
sponsored by the American Institute of Aeronautics and Astronautics
Pasadena, California, January 14-16, 1980

NUMERICAL SIMULATION OF SUPERSONIC INLETS USING A THREE-DIMENSIONAL VISCOUS FLOW ANALYSIS

Bernhard H. Anderson* and Charles E. Towne**
NASA-Lewis Research Center
Cleveland, Ohio

E-325

Abstract

A three-dimensional fully viscous computer analyses, which retains the viscous nature of the Navier-Stokes equations, was evaluated to determine its usefullness in the design of supersonic inlets. This procedure takes advantage of physical approximations to limit the high computer time and storage associated with complete Navier-Stokes solutions. Computed results are presented for a Mach 3.0 supersonic inlet with bleed and a Mach 7.4 Hypersonic inlet. Good agreement was obtained between theory and data for both inlets. Results of a mesh sensitivity study are also shown.

Nomenclature

h_o	total enthalpy
h_1, h_2, h_3	metric coefficients
l_m	mixing length
L_{REF}	reference length (35.56 cm (14 in.) for M3 inlet, 18.33 cm (7.22 in.) for P8 inlet)
m_{BL}	bleed mass flow
m	capture mass flow
M	free-stream Mach number
p	static pressure
p_{REF}	reference pressure (28.5 N/m^2 (58.8 psf) for M3 inlet, 701 N/m^2 (14.6 psf) for P8 inlet)
Re	Reynolds number per unit length based on free-stream (reference) conditions
u_{REF}	reference velocity (640.2 m/sec (2100 ft/sec) for M3 inlet, 1222 m/sec (4008 ft/sec.) for P8 inlet)
u,v,w	velocities in computational coordinates
x,y,z	computational coordinates
x',y'	cartesian coordinates
$\tilde{y}$	distance from wall along computational coordinate
γ	ratio of specific heats
δ_b	boundary layer thickness
κ	Von Karman constant, .43
μ	effective viscosity, laminar + turbulent
μ_T	turbulent viscosity
ρ	density

*Head, Aerodynamics Analysis Section, Member, AIAA
**Aerospace Engineer Member, AIAA

Introduction

The design of three-dimensional supersonic inlets is a difficult task in view of the wide operating range over which good performance is desired. Design of such an inlet system is strongly effected by the requirement that the aircraft operate at all speeds from zero to the supersonic design point. In addition, most supersonic aircraft must have a subsonic cruise capability where fuel economy becomes important. As a result of these varied and sometimes conflicting requirements, the design of supersonic inlets is a difficult compromise.

The foregoing considerations suggest that inlet design technology would benefit from a detailed and accurate flow field calculation procedure that includes shock-boundary layer interaction effects. Within rectangular inlets operating at supersonic speeds, these viscous effects can be classified into three types: (1) incident shock reflections on the centerbody and cowl, (2) glancing shock interactions which take place along the inlet sidewalls, and (3) corner flow interactions. Calculation procedures which are either two-dimensional or do not account for boundary layer effects have limited application towards understanding these viscous interactions.

A number of experimental and analytical papers have been published dealing with these shock interactions. The analysis and comparison with data of an incident shock wave reflection within an axisymmetric inlet have been accomplished by Fukuda, Hingst and Reshotko[1] and Hingst and Towne[2]. In these analyses, control volume methods were used to solve for the properties downstream of the interaction zone given the conditions upstream of the interaction. A similar approach was used by Paynter[3] for the analysis of the weak glancing sidewall interaction. These analyses yield correct trends and represent useful design techniques. An experimental study of the glancing sidewall interaction was done by Oskam, Vas and Bogdonoff[4] and provides a detailed flow description from which to verify analyses. Except for the full Navier-Stokes analysis of the shock-corner boundary layer interaction by Hung and McCormack[5] most of the analyses

of this phenomenon are inviscid[6,7] and provide no information as to the viscous interactions. There are however, a number of experimental reports[8,9] providing data on the viscous corner interaction which are helpful understanding the flow structure itself.

Although full Navier-Stokes procedures would provide the necessary generality to predict the flow within three-dimensional supersonic inlets, the required computer time and storage would be prohibitive in terms of present computer technology. Combined viscous-inviscid interaction analyses of the type suggested by Reyhner and Hickcox[10] for axi-symmetric inlets could be implemented for three-dimensional inlets; however, the coupling procedures would be very complex. An attractive alternative analysis would retain the general three-dimensional viscous nature of the Navier-Stokes equations but would take advantage of physical approximations to limit the high computer run time and storage associated with a complete Navier-Stokes solution. In the present analysis, the assumption if made that there is a primary flow direction and that diffusion in this direction can be neglected. In this manner a set of equations are produced for fully viscous, predominantly supersonic, three-dimensional flow which can be solved by an efficient forward marching technique.

This paper represents the first in a series of studies to evaluate the marching analysis of Buggeln, Kreskovsky, and McDonald[11], designated PEPSIS, and to determine its usefulness in the design of supersonic inlets. Two inlets were chosen for this study; a Mach 3.0 configuration[12] which obtains its compression by means of a crossed shock structure, and a Mach 7.4 hypersonic inlet[13]. Efforts to date have concentrated primarily on the ramp/cowl shock wave boundary layer interactions.

Governing Equations

In this study, the inlet flow field is computed by a spatial marching method[11,14] which solves a simplified form of the three-dimensional Navier-Stokes equations. A curvilinear orthogonal coordinate system is used with coordinate directions x, y, and z and corresponding metric coefficients h_1, h_2, and h_3. Here x is defined as the streamwise or marching direction, and y and z are the two cross-flow directions. The equations are first time-averaged so that they apply to both laminar and turbulent flow. Viscous terms are simplified by using an order-of-magnitude analysis. In particular, in order to allow the use of a marching procedure, x-direction diffusion terms are neglected. The resulting equations are:

Continuity

$$\frac{\partial}{\partial x}(h_2h_3\rho u) + \frac{\partial}{\partial y}(h_1h_3\rho v) + \frac{\partial}{\partial z}(h_1h_2\rho w) = 0$$

x - Momentum

$$\frac{\partial}{\partial x}(h_2h_3\rho u^2) + \left[\frac{\partial}{\partial y} + \frac{1}{h_1}\frac{\partial h_1}{\partial y}\right](h_1h_3\rho uv) + \left[\frac{\partial}{\partial z} + \frac{1}{h_1}\frac{\partial h_1}{\partial z}\right](h_1h_2\rho uw) - h_3\frac{\partial h_2}{\partial x}\rho v^2 - h_2\frac{\partial h_3}{\partial x}\rho w^2 + h_2h_3\frac{\partial p}{\partial x} = \frac{\partial}{\partial y}\left(\frac{h_1h_3}{h_2}\mu\frac{\partial u}{\partial y}\right) + \frac{\partial}{\partial z}\left(\frac{h_1h_2}{h_3}\mu\frac{\partial u}{\partial z}\right)$$

y - Momentum

$$\left[\frac{\partial}{\partial x} + \frac{1}{h_2}\frac{\partial h_2}{\partial x}\right](h_2h_3\rho uv) + \frac{\partial}{\partial y}(h_1h_3\rho v^2) + \left[\frac{\partial}{\partial z} + \frac{1}{h_2}\frac{\partial h_2}{\partial z}\right](h_1h_2\rho vw) - h_3\frac{\partial h_1}{\partial y}\rho u^2 - h_1\frac{\partial h_3}{\partial y}\rho w^2 + h_1h_3\frac{\partial p}{\partial y} = \frac{4}{3}\frac{\partial}{\partial y}\left(\frac{h_1h_3}{h_2}\mu\frac{\partial v}{\partial y}\right) + \frac{\partial}{\partial z}\left(\frac{h_1h_2}{h_3}\mu\frac{\partial v}{\partial z}\right)$$

z - Momentum

$$\left[\frac{\partial}{\partial x} + \frac{1}{h_3}\frac{\partial h_3}{\partial x}\right](h_2h_3\rho uw) + \left[\frac{\partial}{\partial y} + \frac{1}{h_3}\frac{\partial h_3}{\partial y}\right](h_1h_3\rho vw) + \frac{\partial}{\partial z}(h_1h_2\rho w^2) - h_2\frac{\partial h_1}{\partial z}\rho u^2 - h_1\frac{\partial h_2}{\partial z}\rho v^2 + h_1h_2\frac{\partial p}{\partial z} = \frac{\partial}{\partial y}\left(\frac{h_1h_3}{h_2}\mu\frac{\partial w}{\partial y}\right) + \frac{4}{3}\frac{\partial}{\partial z}\left(\frac{h_1h_2}{h_3}\mu\frac{\partial w}{\partial z}\right)$$

The energy equation is eliminated by assuming the total entholpy h_0 is constant. The pressure and density are related through the equation of state,

$$p = \frac{\gamma-1}{\gamma}\rho\left[h_0 - \frac{1}{2}(u^2+v^2+w^2)\right]$$

A mixing length turbulence model is used, with

$$\mu_T = \rho \ell_m^2 \left[\left(\frac{1}{h_2}\frac{\partial u}{\partial y}\right)^2 + \left(\frac{1}{h_2}\frac{\partial w}{\partial y}\right)^2 + \left(\frac{1}{h_3}\frac{\partial u}{\partial z}\right)^2 + \left(\frac{1}{h_3}\frac{\partial v}{\partial z}\right)^2\right]^{1/2}$$

The mixing length distribution is given by:

$$\ell_m(\tilde{y}) = 0.098\delta_b \tanh\left[\kappa\tilde{y}/(0.098\delta_b)\right]$$

The above equations are solved by starting at the ramp tip and marching downstream using an alternatign-direction implicit technique. In this study, to avoid resolving the laminar sublayer, wall function boundary conditions were used to compute tangential velocities on all solid surfaces. Details of the solution procedure are published elsewhere[11,14-16].

In the above equations, the metric coefficients can be computed by any available method. For this study, since only inlets with rectangular cross-sections and parallel sidewalls are considered, h_1 and h_2 are functions of x and y only, and $h_3 = 1$. The mesh was therefore generated using the two-dimensional method of Anderson[17].

Test Cases

In order to evaluate the computational procedure described, two test cases were run with the PEPSIS analysis. The first configuration considered was a large scale, variable geometry, mixed compression inlet[12] designed for Mach 3.0 and a Reynolds number per meter of $7.2\text{X}10^6$ ($2.2\text{X}10^6$ per foot). This test configuration was designated the M3 inlet configuration. It was chosen to study the behavior of the PEPSIS analysis under conditions of high Reynolds number and with a complex crossed shock wave pattern in a largely inviscid core. The second case was a Mach 7.4 hypersonic inlet[13] designated the P8 inlet. This case was chosen to study the behavior of the PEPSIS analysis under conditions of strong shock wave interactions with thick boundary layers. In addition, this inlet was used by Knight[18] as a test case for a two-dimensional Navier-Stokes solution. Each inlet configuration was run with two computational mesh distributions, Table I, designated the coarse and medium mesh solutions. The coarse mesh had 20 grid points distributed between the ramp and cowl surfaces while the medium mesh had 45 grid points. The mesh points for both the coarse and medium mesh solutions were packed in the region near the ramp and cowl surfaces to resolve the wall boundary layers. In this study, since only 6 mesh points were used between the inlet sidewall and the symmetry plane, the sidewall boundary layers were not resolved. This did not lead to any computational problems, however. For both inlets, the streamwise step size distribution was the same for the coarse and medium mesh. Later steps in the evaluation procedure will study the effects of varying the spanwise and streamwise mesh size. The total computing times, i.e., CPU plus I/O time, on the UNIVAC 1100/42 are also listed in Table I.

M3 Inlet Configuration

A schematic diagram of the M3 inlet configuration showing the inviscid shock structure is presented in figure (1). The inlet capture area was 1264 cm^2 (196 in^2) and the initial ramp was inclined 7 degrees to the horizontal. The second ramp was inclined 14 degrees to the horizontal while the cowl surface was parallel to the horizontal. The inlet achieves internal compression by means of a crossed shock structure as indicated in figure (1). Calculations were made on the M3 inlet with the ramp, cowl and sidewall bleed regions shown in figure (2). The bleed rates were computed from the data for configuration 80 of reference 12 and are listed in Table II. A comparison between the coarse and medium meshes used in the calculation of the M3 inlet configuration is shown in figure (3). A section upstream on the ramp tip was added to properly resolve the initial ramp shock in the calculations. In the description that follows, u and v are the streamwise and cross-flow velocities in this coordinate system. In addition, the gapwise distance is defined as the distance along a coordinate line from the ramp to the cowl. Comparisons between the coarse and medium mesh solutions are presented in figures (4)-(6). In figure (4), computed Mach number profiles in the center plane of the M3 inlet have been plotted within the inlet geometry. The coarse mesh solution exhibited substantial numerical noise, particularly in those regions where an oblique shock either formed or was reflected from a solid surface. This can be seen more clearly in figure (5) where the u-velocity (streamwise velocity) profiles have been plotted as a function of normalized gap distance across the flow field. Differences in the computed shock wave structure are also evident in figure (5). A more distinct second ramp shock is apparent in the medium mesh solution in addition to an upstream shift in the first ramp shock-boundary layer interaction. The dramatic differences between the coarse and

medium mesh solutions can also be seen in figure (6) which presents the v-velocity (normal velocity) profiles in the M3 inlet center plane as a function of normalized gap distance. The v-velocity is very sensitive to mesh resolution and it is evident from figure (6) that the numerical problems encountered in the coarse mesh solution were essentially eliminated in the medium mesh solutions.

A comparison between the two solutions and experimental static pressure measurements is presented in figure (7). The medium mesh gave a forward shift in the shock-boundary layer interactions, but both solutions agree well with the data. The boundary layers on both the ramp and cowl surface were thin relative to the channel gap dimensions so that detailed resolution of these interactions would require additional mesh points. The solution ended just upstream of the throat because of a substantial region of subsonic flow in the core of the flow field which the PEPSIS analysis cannot presently handle.

In order to continue the solution past this region, a second medium mesh calculation was performed at over speed conditions, i.e., at a free stream Mach number of 3.25, and the results are presented in figure (8). The Mach number profiles which are plotted within the inlet geometry reveal that the shock impinging on the ramp shoulder has been cancelled by the sudden expansion around the shoulder. Compression downstream of the shoulder thus takes place by a single reflected shock system. The increase in boundary layer thickness as a result of the sudden expansion around the ramp shoulder is also evident. Again to properly resolve the flow phenomena in the region of the ramp shoulder would require a much greater mesh density. However, the PEPSIS analysis does simulate the gross features of the flow with the present mesh resolution which makes it ideal for design.

P8 Inlet Configuration

In order to investigate the ability of the PEPSIS analysis to compute the details of the shock wave-boundary layer interactions a series of calculations was made on a Mach 7.4 hypersonic inlet. Under hypersonic conditions, much thicker boundary layers are encountered so that greater resolution of these interactions can be achieved without increasing the number of mesh points.

A schematic diagram of the P8 hypersonic inlet showing the inviscid shock structure is presented in figure (9). The initial ramp angle was inclined 6.45 degrees to the horizontal while the initial cowl angle was inclined -1 degree to the horizontal. The leading edge of the cowl on the P8 inlet was blunt, with a diameter of 0.114 cm (.0449 in). Since it is impractical to resolve this blunt body flow in a complete inlet analysis an effective sharp cowl leading edge was defined. Using the expressions from Hayes and Probstein[19] for two-dimensional shock standoff distance, and positioning the initial cowl shock tangent to the bow lip shock, figure (10), gave an effective displacement of 0.26 cm (.10 in). This compares to an effective cowl lip displacement of 2.8 cm (1.1 in) used in the two-dimensional Navier-Stokes solution of this inlet by Knight[18].

A comparison between the coarse and medium mesh Mach number profiles plotted within the inlet geometry is presented in figures (11) and (12). Figure (11) shows the developing Mach number profiles for the entire P8 inlet, while figure (12) presents an enlarged view internal to the inlet. More distinct initial ramp and cowl shock waves are apparent in the medium mesh solution. With the enlarged view of the internal Mach number profile development, figure (12), the cowl shock wave interaction with the thick ramp boundary layer becomes evident. The reflected shocks off both the ramp and cowl boundary layers are also clearly present. Differences between the coarse and medium mesh solutions become more apparent by plotting the Mach number profile development in terms of normalized gap distance across the inlet channel, figure (13). The numerical noise disturbances generated just downstream of both the ramp and cowl shock waves in the coarse mesh solution, figure (13a), are propagated along Mach lines and act like weak shock waves. Increasing the mesh density essentially eliminated these numerical disturbances. The medium mesh solution, figure (13b), had enough grid points to resolve the detailed flow events within the length scale associated with this interaction. The boundary layer buildup along the ramp surface and its interaction with the cowl shock is clearly evident. The static pressure profile development in the center plane of the P8 inlet, figure (14), reveals more clearly that the numerical noise disturbances are propagated along Mach lines in the coarse mesh solution and that increased mesh resolution eliminates these problems. Note also that there is a substantial normal pressure gradient across the ramp and cowl boundary layers within the interaction zone.

Comparisons of the coarse and medium mesh static pressure solutions with measurements in the center plane of the P8 inlet are shown in figure (15). The calculations were performed assuming turbulent boundary layer flow along both the ramp and cowl surfaces while the experimental test had substantial laminar flow on both surfaces.

As a result, the analysis predicted a thicker boundary layer entering both interaction regions which resulted in a slight upstream shift in the shock location. In spite of these differences very good static pressure predictions were achi· ved with the PEPSIS analysis. The PEPSIS code is presently being updated to include a laminar-turbulent transition capability. It is expected that with thinner boundary layers still better agreement will be achieved. A comparison between the PEPSIS viscous analysis and inviscid calculations[20] is presented in figure (16) and shows a strong ramp shock interaction extending well upstream of the inviscid shock impingement point and a substantial upstream displacement in the cowl shock interaction region.

Concluding Remarks

A series of calculations were performed on two inlet configurations using a three-dimensional viscous flow analysis (PEPSIS) and the following remarks can be made:

1. With proper overall mesh resolution, the PEPSIS analysis is able to define the basic features of high Reynolds number thin boundary layer flows with highly complex shock wave structures in a largely inviscid core.

2. Even when the solution mesh is too coarse to properly resolve the small length scale events associated with thin boundary layer-shock wave interactions, the overall features of these events can be predicted.

3. With adequate mesh resolution of the shock wave-boundary layer interactions, the PEPSIS analysis predicts the gross physics of this flow event.

4. Depending on the mesh density, the PEPSIS analysis can be used either as a design tool, where the overall inlet flow field is the important factor, or as an analysis tool where the small scale flow events occuring in inlets can be studied.

5. Numerical noise disturbances can develop within the solution which will distort the flow field, but proper mesh resolution can eliminate this problem.

References

1. Fukuda, M.K., Hingst, W.R., and Reshotko, E., "Control of Shock Wave-Boundary Layer Interactions by Bleed in Supersonic Mixed Compression Inlets," Case Western Reserve University, Cleveland, OH, FTAS/TR-75-100, August 1975. (NASA CR-2595)

2. Hingst, W.R., and Towne, C.E., "Comparison of Theoretical and Experimental Boundary Layer Development in a Mach 2.5 Mixed-Compression Inlet," NASA TM X-3026, April 1974.

3. Paynter, G.C., "Analysis of Weak Glancing Shock/Boundary Layer Interactions," AIAA Paper 79-0144, January 1979.

4. Oskam, B., Vas, I.E., and Bogdonoff, S.M., "Mach 3 Oblique Shock Wave/Turbulent Boundary Layer Interactions in Three Dimensions," AIAA Paper 76-336, July 1976.

5. Hung, C.M., and MacCormack, R.W., "Numerical Solution of Three-Dimensional Shock Wave and Turbulent Boundary Layer Interaction," AIAA Journal, Vol. 16, No. 10, October 1978, pp. 1090-1096.

6. Kutler, P., "Numerical Solution for the Inviscid Supersonic Flow in the Corner Formed by Two Intersecting Wedges," AIAA Paper 73-675, July 1973.

7. Marconi, F., "Internal Corner Flow Fields," AIAA Paper 79-0014, January 1979.

8. Cooper, J.R., and Hankey, W.L. Jr., "Flow Field Measurements in an Axisymmetric Axial Corner at M = 12.5," AIAA Journal, Vol. 12, No. 10, October 1974, pp. 1353-1357.

9. West, J.E., and Korkegi, R.H., "Interaction in the Corner of Intersecting Wedges at a Mach Number of 3 and High Reynolds Numbers," Aerospace Research Labs, Wright Patterson AFB, Ohio, ARL 71-0241, October 1971. (AD-734540)

10. Reyhner, T.A., and Hickcox, T.E., "Combined Viscous-Inviscid Analysis of Supersonic Inlet Flowfields," Journal of Aircraft, Vol. 9, No. 8, August 1972, pp. 589-595.

11. Buggeln, R.C., Kreskovsky, J.P., and McDonald, H., "Computation of Three-Dimensional Viscous Supersonic Flow in Inlets," AIAA Paper 80-0194, January 1980.

12. Anderson, W.E., and Wong, N.D., "Experimental Investigation of a Large Scale, Two-Dimensional, Mixed-Compression Inlet System - Performance at Design Conditions, M_{∞} = 3.0," NASA TM X-2016, May 1970.

13. Gros, A.V., Watson, E.C., Seebough, W.R., Sanator, R.J., and DeCarlo, J.P., "Investigation of Flow Fields Within Large Scale Hypersonic Inlet Models," NASA TN D-7150, April 1973.

14. Buggeln, R.C., McDonald, H., Kreskovsky, J.P., and Levy, R., "Development of a Three-Dimensional Supersonic Inlet Flow Analysis," NASA CR-3218, Nov. 1979.

15. Briley, W.R., Kreskovsky, J.P., and McDonald, H., "Computation of Three-Dimensional Viscous Flow in Straight and Curved Passages," United Technologies Research Center, East Hartford, CT, R76-911841-9, August 1976.

16. McDonald, H., and Briley, W.R., "Three-Dimensional Supersonic Flow of a Viscous or Inviscid Gas," Journal of Computational Physics, Vol. 19, No. 2, October 1975, pp. 150-178.

17. Egolf, T.A., Anderson, O.L., Edwards, I.E., and Landgrebe, A.J., "An Analysis for High Speed Propeller-Nacelle Aerodynamic Performance Prediction; Volume 1, Theory and Application," United Technologies Research Center, East Hartford, CT, R79-912949-19, June 1979.

18. Knight, D.D., "Numerical Simulation of Realistic High Speed Inlets Using the Navier-Stokes Equations," AIAA Journal, Vol. 15, No. 11, November 1977, pp. 1583-1589.

19. Hayes, W.D., and Probstein, R.F., Hypersonic Flow Theory, Vol. 1: Inviscid Flows, 2nd. ed., Academic Press, New York, 1966, pp. 232-245.

20. Anderson, B.H., Tassa, Y., and Reshotko, E., "Characteristics Procedure for Supersonic Flows Including Consideration of Viscous Contributions to Flow Rotationality," AIAA Paper 76-426, July 1976.

TABLE I. - TEST CASES FOR PEPSIS

Test cases	Computational mesh		Computing time* on UNIVAC 1100/42, min
	Distribution	Total	
M3 inlet			
Coarse	20×6×180	21 600	58
Medium	45×6×177	47 790	129
Medium	45×6×260	70 200	190
P8 inlet			
Coarse	20×6×350	42 000	113
Medium	45×6×340	91 800	248

*CPU plus I/O time.

TABLE II. - BLEED RATES FOR M3

INLET CONFIGURATION

Bleed zone	Bleed mass flow, $\dot{m}_{BL}/\dot{m}_{\infty}$	Bleed velocity, v/u_{ref}
R_A	0.0097	0.00902
R_B	.0053	.00528
R_C	.0193	.00769
R_D	.0214	.00832
C_A	.0120	.00295
C_B	.0699	.00431
S_A	.0120	.00451
S_B	.0147	.00748
S_C	.0176	.01277

$\dot{m}_{\infty}$ = 7.006 kg/sec (15.45 lb_m/sec).

u_{ref} = 640.2 m/sec (2100 ft/sec).

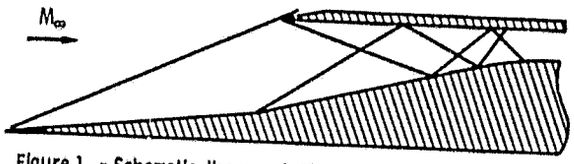

Figure 1. - Schematic diagram of M3 inlet configuration showing inviscid shock structure.

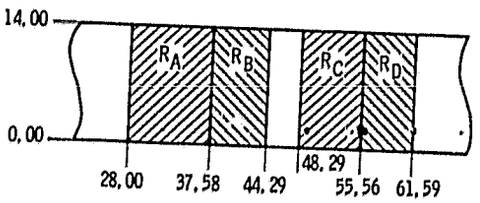

(a) RAMP.

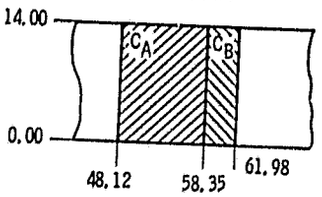

(b) COWL.

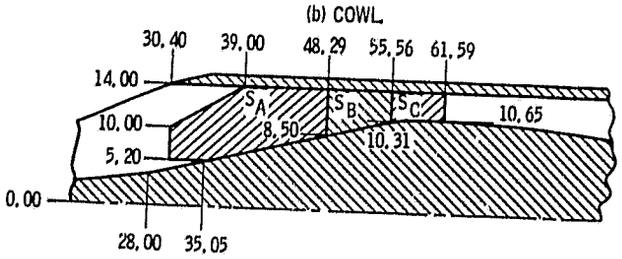

(c) SIDEWALL.

Figure 2. - Bleed regions for M3 inlet configuration. (Distances are model stations from ref. 12.)

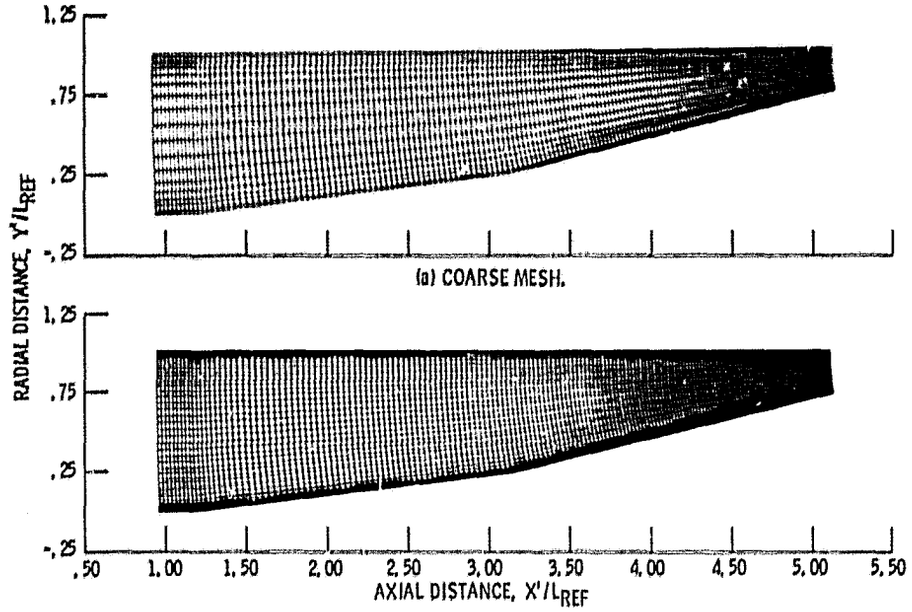

Figure 3. - Comparison of coarse and medium mesh used in computation of M3 inlet flow field.

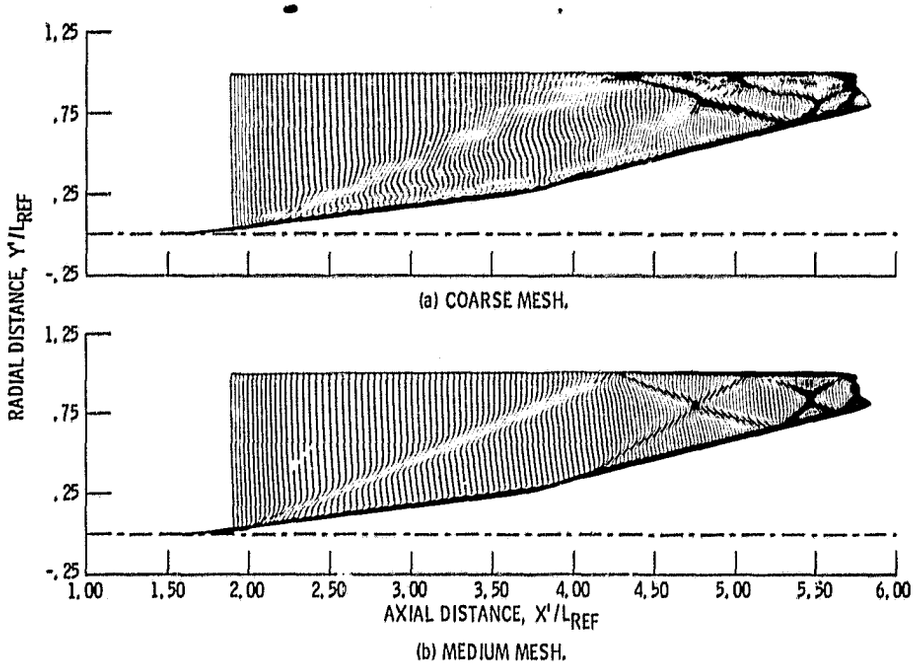

Figure 4. - Mach number profiles in center plane of M3 inlet configuration. $M_\infty = 3.0$; Re = 7.2×10^6/m (2.2×10^6/ft).

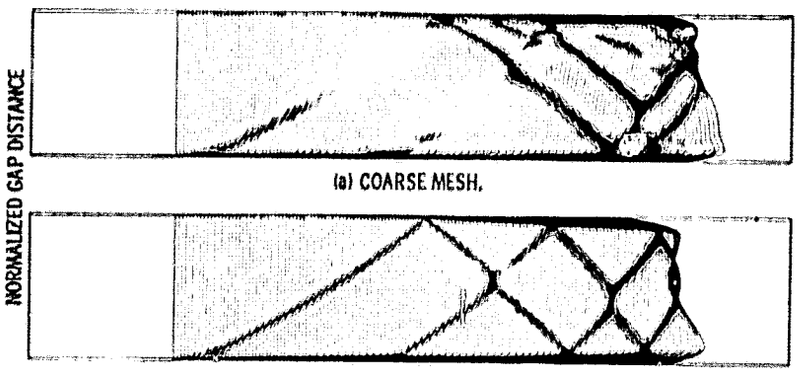

Figure 5. - Effect of mesh on the u-velocity profiles in center plane of M3 inlet configuration.

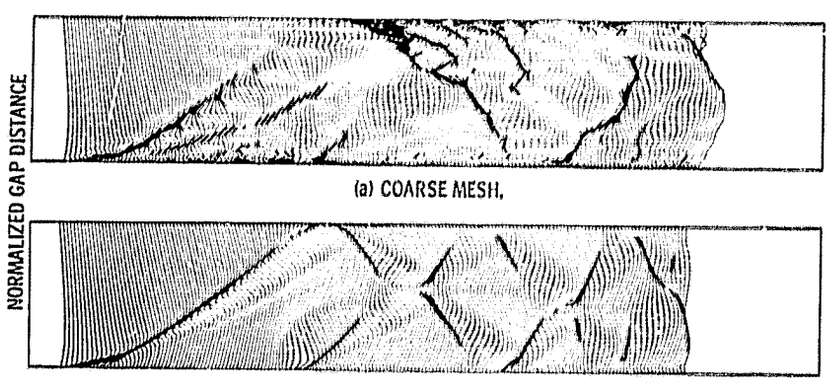

Figure 6. - Effect of mesh on the v-velocity profiles in center plane of M3 inlet configuration.

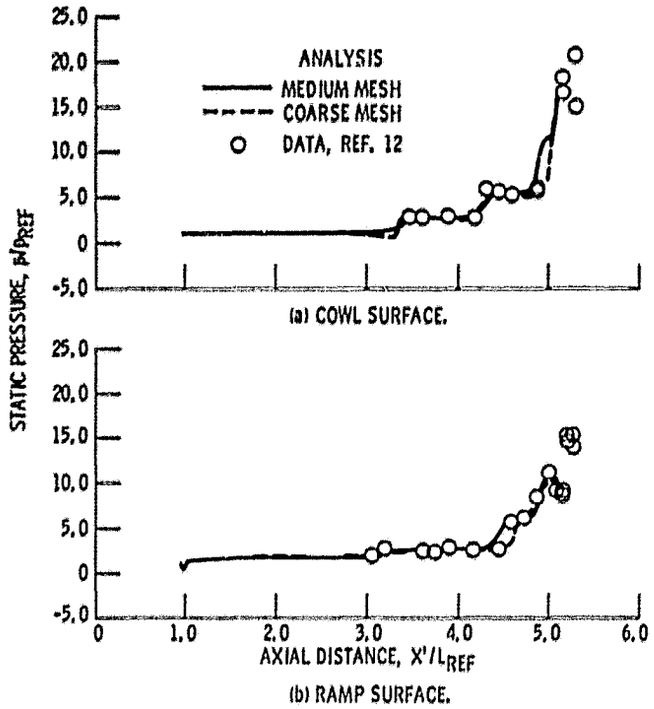

(a) COWL SURFACE.

(b) RAMP SURFACE.

Figure 7. - Effect of mesh on the wall static pressure distribution in center plane of M3 inlet configuration.

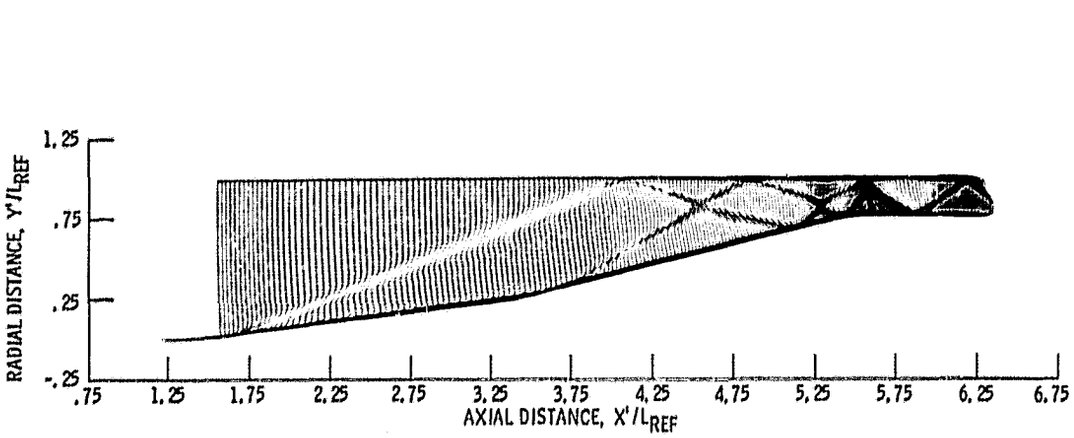

Figure 8. - Medium mesh flow field solution for M3 inlet configuration at overspeed conditions, $M_\infty = 3.25$.

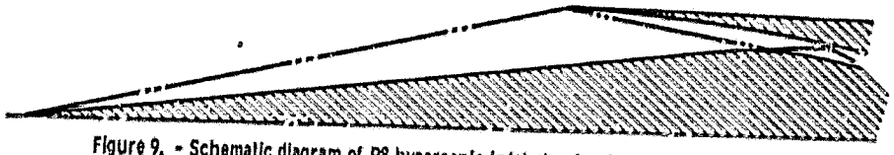

Figure 9. - Schematic diagram of P8 hypersonic inlet showing inviscid shock structure.

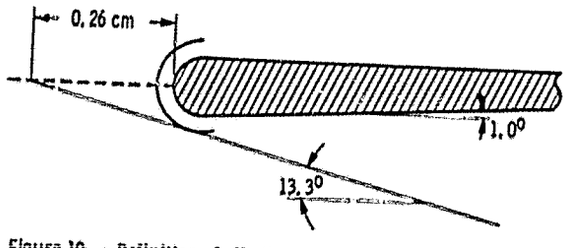

Figure 10. - Definition of effective cowl leading edge (not to scale).

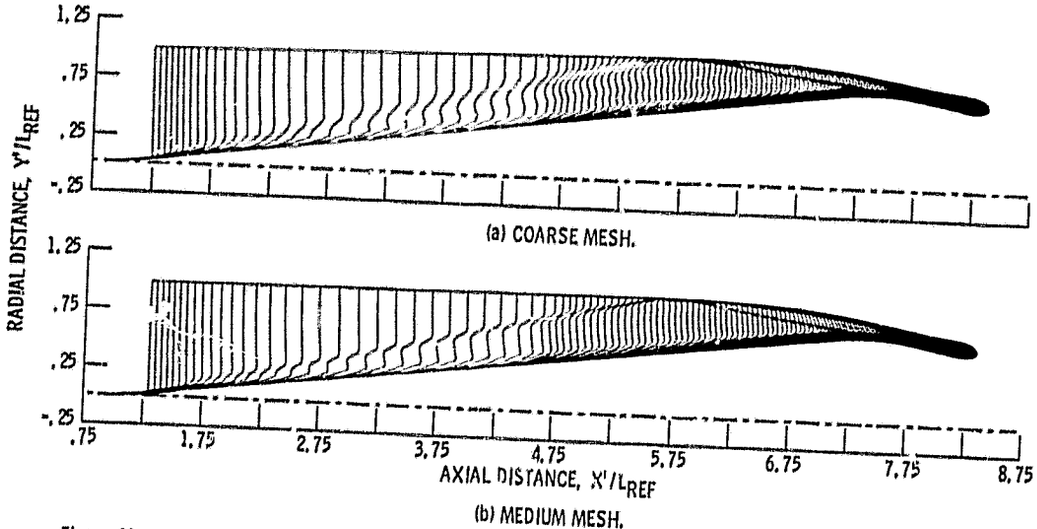

Figure 11. - Mach number profiles in center plane of P8 inlet configuration. $M_\infty = 7.4$; $Re = 8.9 \times 10^6$/m (2.7×10^6/ft).

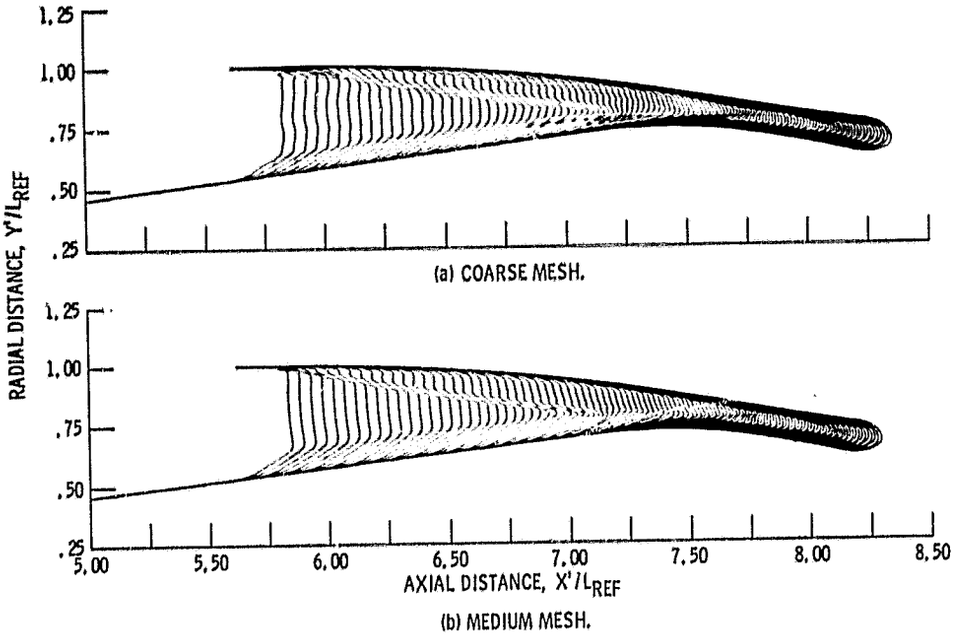

Figure 12. - Internal Mach number profiles in center plane of P8 inlet configuration. $M_\infty = 7.4$; Re = 8.9×10^6/m (2.7×10^6/ft).

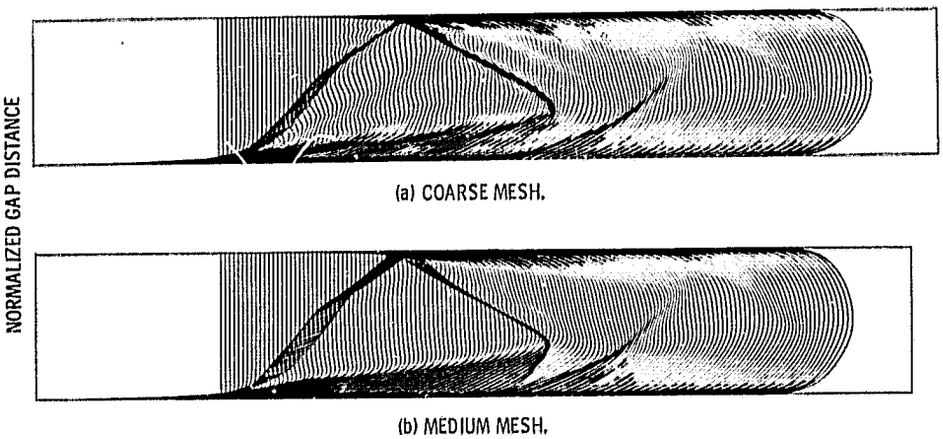

Figure 13. - Effect of mesh on Mach number profiles in center plane of P8 inlet configuration.

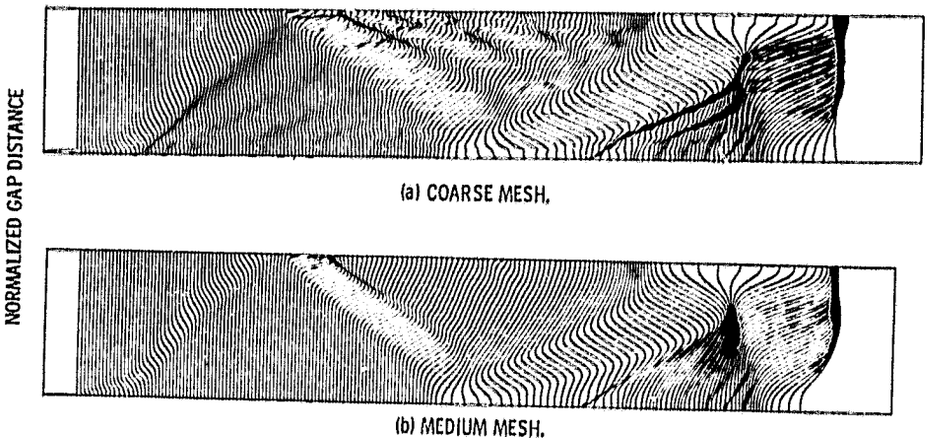

(a) COARSE MESH.

(b) MEDIUM MESH.

Figure 14. - Effect of mesh on static pressure profiles in center plane of P8 inlet configuration.

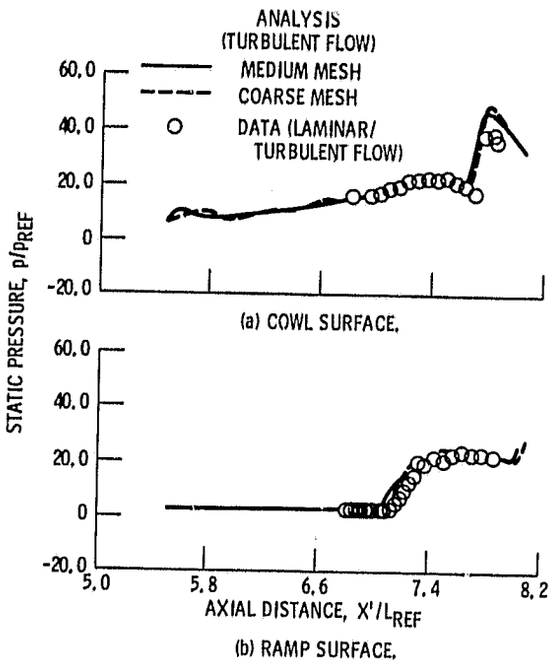

(a) COWL SURFACE.

(b) RAMP SURFACE.

Figure 15. - Effect of mesh on wall static pressure distribution in center plane of P8 inlet configuration.

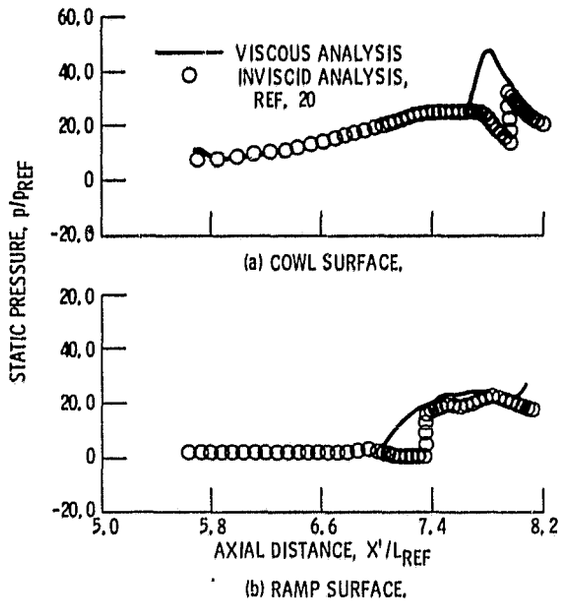

Figure 16. - Comparison of medium mesh viscous solution with inviscid analysis for wall static pressure in center plane of P8 inlet configuration.

1. Report No. NASA TM-81411	2. Government Accession No.	3. Recipient's Catalog No.
4. Title and Subtitle NUMERICAL SIMULATION OF SUPERSONIC INLETS USING A THREE-DIMENSIONAL VISCOUS FLOW ANALYSIS		5. Report Date 6. Performing Organization Code
7. Author(s) B. H. Anderson and C. E. Towne		8. Performing Organization Report No. E-325 10. Work Unit No.
9. Performing Organization Name and Address National Aeronautics and Space Administration Lewis Research Center Cleveland, Ohio 44135		11. Contract or Grant No.
12. Sponsoring Agency Name and Address National Aeronautics and Space Administration Washington, D.C. 20546		13. Type of Report and Period Covered Technical Memorandum 14. Sponsoring Agency Code
15. Supplementary Notes		

16. Abstract

A three-dimensional fully viscous computer analysis, which retains the viscous nature of the Navier-Stokes equations, was evaluated to determine its usefulness in the design of supersonic inlets. This procedure takes advantage of physical approximations to limit the high computer time and storage associated with complete Navier-Stokes solutions. Computed results are presented for a Mach 3.0 supersonic inlet with bleed and a Mach 7.4 hypersonic inlet. Good agreement was obtained between theory and data for both inlets. Results of a mesh sensitivity study are also shown.

17. Key Words (Suggested by Author(s))

Supersonic inlet
Parabolized Navier-Stokes
Shock waves
Viscous flow
Marching analysis

18. Distribution Statement

Unclassified - unlimited
STAR Category 34

19. Security Classif. (of this report)	20. Security Classif. (of this page)	21. No. of Pages	22. Price*
Unclassified	Unclassified		

* For sale by the National Technical Information Service, Springfield, Virginia 22161